euspen's 25th International Conference & Exhibition, Zaragoza, ES, June 2025
www.euspen.eu

Binocular Single-frequency Fringe Projection Profilometry for Measuring Metal Additively Manufactured Parts

Lifei Ren[1], Chi Fai Cheung[1], Ho Lai Ting[1], Da Li[1,2]

[1] *State Key Laboratory of Ultra-precision Machining Technology, Department of Industrial and Systems Engineering, The Hong Kong Polytechnic University, Hung Hom, Kowloon, Hong Kong, China*
[2] *Institute of Modern Optics, Nankai University, Tianjin, China*

benny.cheung@polyu.edu.hk

Abstract
Binocular fringe projection profilometry is widely utilized in industrial 3D surface measurements due to its advantages of high precision, efficiency, low cost, and simple structure. This paper presents a 3D measurement system based on binocular fringe projection profilometry for measuring metal additive manufacturing parts. The system comprises two industrial cameras and a structured light projector, which requires only the projection of three-step single-frequency fringe patterns to acquire the 3D point cloud of the measured parts. The wrapped phase maps are extracted from the three-step phase shift images of the binocular cameras. Then, they are unwrapped using the geometric constraints in the imaging and projecting process without the requirements of projecting additional fringe patterns. The unwrapped phase maps are then stereo-matched to compute the disparity map and reconstruct the 3D point cloud of the measured surface. Experimental results demonstrate that the proposed system achieves high precision and reliability in measuring metal additive manufacturing parts, making it a promising solution for industrial applications requiring accurate 3D surface measurements.

Fringe projection profilometry, 3D metrology, Precision Measurement

1. Introduction

Metal additive manufacturing (AM) has revolutionized the production of complex and high-performance components by enabling layer-by-layer fabrication with enhanced design flexibility [1, 2]. Various AM techniques, such as sintering-based AM [3], friction stir-based AM [4], wire arc AM [5], and selective laser melting (SLM) [6], offer distinct advantages in terms of microstructure refinement, density control, and manufacturing efficiency. Among these, SLM, a typical powder bed fusion technology, uses a high-powered laser to fuse layers of metal powder. After printing, parts are removed from the powder bed and separated from the build plate. SLM is particularly notable for achieving fine microstructures and high precision, making it suitable for applications requiring tight tolerances. However, ensuring AM-fabricated components' dimensional accuracy and surface quality remains a critical challenge. Advanced 3D metrology techniques are essential for tolerance verification and quality assurance [7].

3D measurement technologies are broadly categorized into contact and non-contact methods. Contact-based methods offer high accuracy and can measure surfaces with steep slopes, but they risk damaging the surface and are time-consuming due to point-by-point scanning. Non-contact optical methods [8] overcome these limitations and are divided into interferometric and non-interferometric techniques. Interferometric methods [9] achieve sub-micrometric resolution but are sensitive to environmental disturbances like temperature changes, aerodynamic turbulence and vibrations. Among non-interferometric methods, stereo vision [10] is the most popular for 3D shape metrology and is further divided into passive and active approaches. Passive stereo vision relies on binocular stereo matching, which works well only on textured surfaces, limiting its industrial applications. On the other hand, active stereo vision uses structured light patterns or laser illumination, making it widely applied in industrial inspection.

Fringe Projection Profilometry (FPP) [11-13] is a widely used active stereo vision technique in manufacturing [14, 15], materials science [16, 17], reverse engineering [18, 19], and biomedical engineering [20, 21] due to high precision, non-contact measurement capabilities, and a relatively simple system structure. Several studies have applied FPP to inspect AM parts. Zhang et al. [22] developed an FPP system with a modified sensor model and improved phase unwrapping for powder bed fusion. Using FPP, Liu et al. [29] proposed an in-situ metrology technique for Electron Beam Powder Bed Fusion. Shi et al. [23] introduced a phase correction method in 3D sampling moiré profilometry for residual stress analysis during AM. The complex geometries of AM parts with large slope and inevitable image noise from projection and imaging pose challenges for 3D metrology. To address these issues, this paper presents a binocular FPP system with a single-frequency fringe for inspecting metal AM parts, which utilizes phase-based stereo matching to enhance algorithm robustness, effectively mitigate imaging noise caused by the complexity of AM parts and feature variations due to illumination changes, thereby improving matching accuracy and stability. Additionally, this method eliminates the need for extra fringe projections required in time-domain phase unwrapping, thus enhancing measurement efficiency. The accuracy of the constructed 3D measurement system based on binocular FPP was evaluated using a standard artefact. The system was then applied to measure metal AM parts, obtaining 3D point cloud data of the parts. The point cloud data was matched and analysed against the digital models of the parts, verifying the effectiveness of the built 3D measurement system for inspecting metal AM parts. The remainder of the paper is organized as follows: Section 2 will illustrate the principle of binocular FPP and describe the phase unwrapping

method based on the geometric constraints in binocular FPP. Section 3 conducts measurement experiments, including evaluating the measuring precision and verifying the application of additively manufactured parts using binocular FPP. Section 4 will summarize conclusions of this paper.

2. Principle of binocular FPP with single-frequency fringe

A measurement system based on binocular FPP comprises two industrial cameras and a projector that projects sinusoidal fringe patterns. Before performing measurements, the entire measurement system must be calibrated to obtain the projection matrices that map 3D points in the world coordinate system to image points on the imaging planes of the two cameras and the projector. This calibration lays the foundation for the subsequent reconstruction of 3D point clouds.

Figure 1 illustrates the principle of binocular FPP with single-frequency fringes. The measurement process is described as follows: the projector projects three sinusoidal fringe patterns with different phase shifts onto the object being measured. The two cameras capture the deformed fringe patterns modulated by the object. From these images, phase maps are extracted to obtain wrapped phase maps for both the left and right cameras. A phase unwrapping algorithm is used to the wrapped phase maps to obtain absolute phase maps. Using the calibration results, stereo rectification is performed on the images from the two cameras, aligning the epipolar lines horizontally, which allows the system to search for the closest matching point in the horizontal direction of the right camera's phase map for each point in the left camera's phase map, thereby generating a disparity map. Finally, the disparity map is converted into a 3D point cloud using triangulation based on the calibration results.

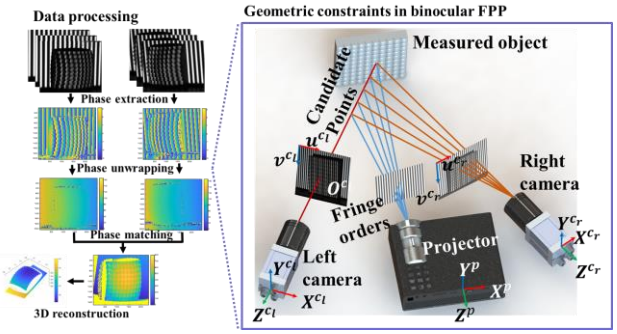

Figure 1. Schematic diagram of binocular FPP with single-frequency fringe

The phase unwrapping algorithm in this process eliminates phase ambiguity, which can introduce errors in stereo matching. Typical phase unwrapping methods, such as temporal phase unwrapping techniques like multi-frequency heterodyne methods, require projecting multiple sets of fringe patterns with different frequencies, which reduces measurement efficiency and increases errors caused by object motion during image acquisition. This paper proposes a method to achieve phase unwrapping without projecting additional fringe patterns by analysing the geometric constraints between the binocular cameras and the projector in the binocular FPP system. Figure 1 shows the geometric constraints in the binocular FPP system. For a point on the left camera's image, different fringe orders correspond to different candidate 3D points in space. These relationships can be determined using the geometric relationship between the cameras and the projector. Each set of candidate 3D points' corresponding phase values can be projected onto the right camera's image. The correct fringe order can be determined by identifying the phase value on the right camera that is closest to the phase value on the left camera. To enhance the algorithm's robustness, we construct an energy function for all pixels in the left camera's image based on the above principle. A regularization term is introduced, and the problem is formulated as a Markov Random Field (MRF) model. By solving this model, the fringe orders for the entire image are determined, enabling phase unwrapping without the need for additional fringe patterns. After phase unwrapping, stereo matching is performed to generate the disparity map, which is then converted into a 3D point cloud.

3. Metrology of metal additively manufactured parts

3.1 Measurement system

A 3D surface measurement system based on binocular FPP was constructed to measure metal AM parts, as shown in Figure 2. The technical specifications of the measurement system are listed in Table 1. The measurement system consists of two industrial cameras (Daheng MER-503-36U3M) with a resolution of 2448 × 2048, telecentric lenses (Moritex MML05-HR65) paired with the cameras, and a structured light projector (Texas Instruments DLP4500) with a resolution of 912 × 1140. The system operates at a working distance of approximately 56.6 mm, with a field of view of 34.0 mm × 28.4 mm and a measurement depth range of 16 mm. The left and right cameras are synchronized, and the system was fully calibrated before measurement, resulting in a reprojection error of 0.1015 pixels.

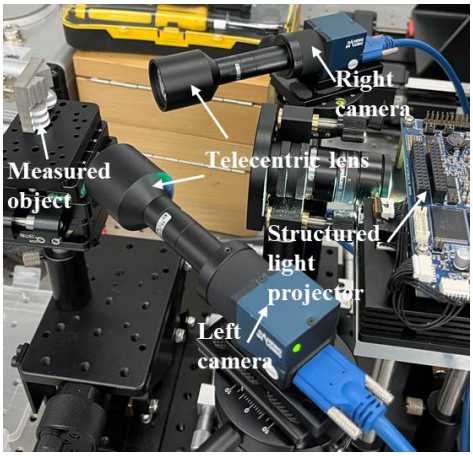

Figure 2. Measurement system using binocular FPP

Table 1 Technical specification of the measurement system using binocular FPP

Work distance	$56.6mm$
Depth range	$16mm$
Field of view	$34.0mm \times 28.4mm$
CMOS resolution	2448×2048
DLP resolution	912×1140
Video FPS	12
XY resolution	$6.9\mu m$
Precision	$8.0\ \mu m$
Dimension	$300mm \times 300mm \times 230mm$
Light source	LED blue illumination
Connector	USB3.0

3.2 Measurement precision analysis

Before measuring the AM parts using the built measurement system, we first evaluated the system's measurement accuracy using a calibration artefact composed of three standard ceramic spheres with a diameter of 5 mm. The CAD model of the

calibration artefact and the spatial distribution of the three spheres are shown in Figure 3(a). The centre-to-centre distances of the spheres are denoted as Dist1, Dist2, and Dist3, while the radii of the spheres are denoted as R1, R2, and R3. Figure 3(b) shows the photograph of the artefact. Using the proposed measurement system, a disparity map of the calibration artefact was obtained, as shown in Figure 3(c), which was then converted into a 3D point cloud of the three standard spheres, as shown in Figure 3(d). In the 3D point cloud, the colour represents the fitting error map obtained by performing spherical fitting on the 3D point cloud of the three standard spheres. The mean absolute errors (MAD1, MAD2, MAD3) and root mean square errors (RMS1, RMS2, RMS3) of the fitting results were calculated to evaluate the system's accuracy.

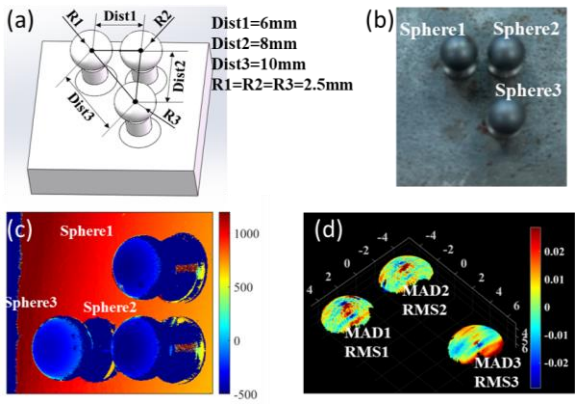

Figure 3. Three-sphere calibration artefact: (a) CAD model and dimensions; (b) photograph; (c) disparity map; (d) Point cloud and spherical fitting error map

Using the proposed 3D measurement system, the calibration artefact was measured five times at different positions and poses. Figure 4 illustrates the deviations of the sphere centre-to-centre distances, sphere radii, and the spherical fitting errors (mean absolute error and root mean square error) from their nominal values during the five measurements. Statistical analysis reveals that the average measurement errors for the sphere center-to-center distances and sphere radii are 2.5 µm and 3.1 µm, respectively. The mean absolute error and root mean square error of the spherical fitting are 6.3 µm and 8.0 µm, respectively. The proposed measurement system meets the required precision standards because most metal AM applications require sub-millimeter measurement accuracy.

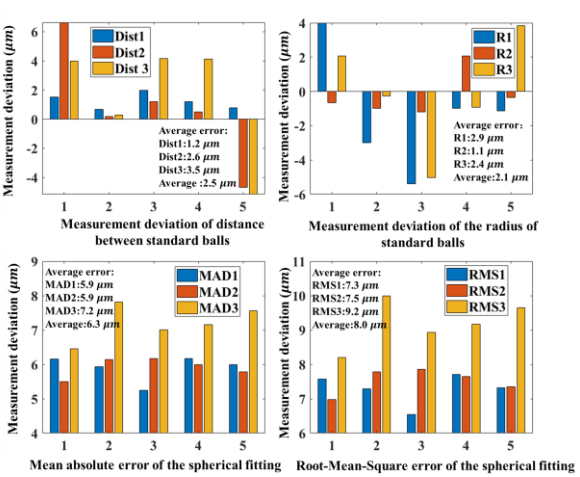

Figure 4. Measurement deviation of different dimensions and spherical fitting errors of three-sphere calibration artefact

3.3 Metrology of metal additively manufactured parts

This study used the built measurement system based on BFPP to inspect the surface of parts manufactured using metal AM technology. The experiments were conducted using the powder-bed laser 3D printer (HANS-M-100) developed by Han's Laser Technology Industry Group Co., Ltd, as shown in Figure 5. The material used was 316L stainless steel. The technical specifications of the metal 3D printer are listed in Table 2. The forming accuracy of this metal 3D printer can reach 0.1 mm. However, the actual accuracy depends on factors such as the machine's operating condition, printing material, printing parameters (layer height, laser intensity, printing speed), powder layer thickness, and working temperature.

Figure 5. Photograph of laser 3D printer HANS-M-100

Table 2 Technical specification of laser 3D printer HANS-M-100

Dimension	1000mm × 1000mm × 1900mm
Maximum forming size	110mm × 110mm × 100mm
Forming precision	±0.05mm
Laser power	500W
Beam quality	$M^2 < 1.1$
Laser wavelength	1060nm~1080nm
Beam diameter	$\leq 55\mu m$
Layer thickness	$20\mu m$~$100\mu m$
Optical lens	F-theta-lens
Scanning speed	≤10m/s
Oxygen content	$\leq 100ppm$
Flour feeding method	Downfeed
Gas shield	Nitrogen/Argon
Software	Magics
Power	200V±10%，30A/≤5KW
Material	Stainless steel, die steel, super alloy, titanium alloy, aluminum alloy, etc
Control	Profinet

To ensure the quality of the manufactured parts, it is necessary to measure the processed parts to obtain 3D point cloud data of their surfaces. The point cloud data is then matched and analysed against the 3D model of the part. By comparing the measured data with the 3D model, it is possible to verify whether the manufactured parts meet the design requirements and to analyze the manufacturing errors.

In this study, four parts, including a triangular prism, a hemispheroid, a spherical lens array, and a spherical lens array on a convex substrate, as shown in Figures 6(a) and (b), are measured. The 3D point clouds of measured surface obtained from the measurement system are shown in Figure 6(c).

To further analyze the 3D measurement results, the point clouds of the four parts are matched with their respective 3D

models to evaluate whether the manufacturing accuracy meets the design requirements. The error maps and dimensional shape analyses from the CAD-to-measurement comparisons are presented in Figure 7. For the spherical lens array, the measurement deviations for the spherical radius, lateral array dimension, longitudinal array dimension, and form error are -0.095 mm, 0.019 mm, 0.270 mm, and 0.139 mm, respectively, all within the allowable tolerances. For the triangular prism, the flatness errors of the two inclined planes are 0.074 mm and 0.127 mm, and the angular deviation between the two inclined planes is -0.130°, all within the allowable tolerances. For the hemispheroid, the sphericity error is 0.131 mm, and the deviation of the spherical centre is -0.0376 mm, and the flatness error of the substrate is 0.223 mm, all within the allowable tolerances. The form error for the spherical lens array on a convex substrate is 0.192 mm, which also fall within the allowable tolerances.

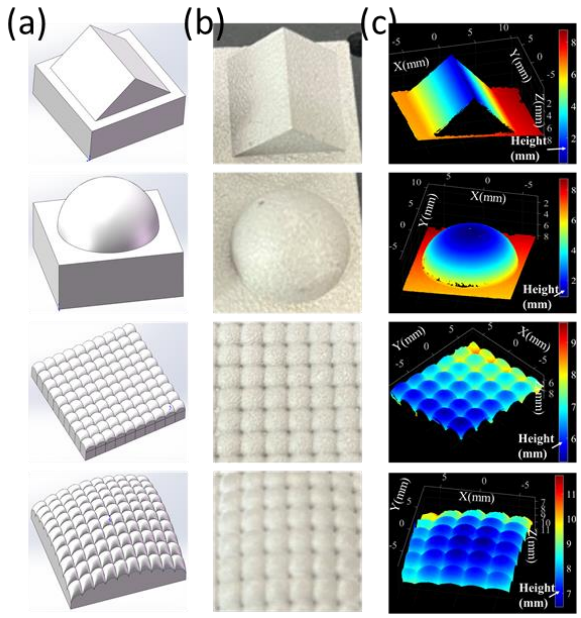

Figure 6. Measurement results of metal additively manufactured parts: (a) CAD models; (b) photographs; (c) point clouds

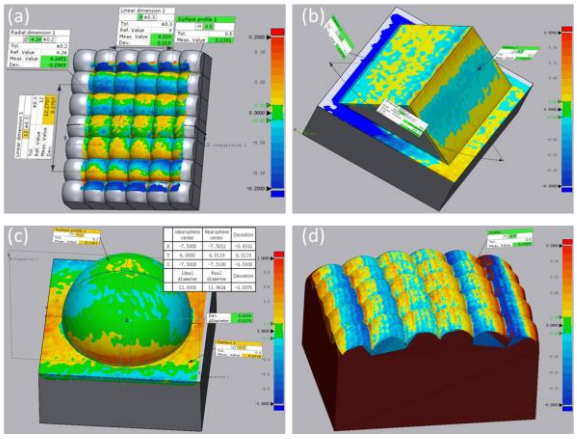

Figure 7. Measurement data analysis of spherical lens array: (a) spherical lens array; (b) triangular prism; (c) hemispheroid; (d) spherical lens array on a convex substrate

4. Conclusions

This paper presents a binocular FPP system with single-frequency fringe for measuring metal parts fabricated through AM. The phase unwrapping processes are conducted based on the geometric constraints in binocular FPP without the requirement of projecting additional fringe patterns. Experimental results confirm that the developed binocular FPP is well-suited for inspecting complex geometries of metal AM parts. The system's accuracy was evaluated by measuring a standard artefact. The developed system achieves a measurement accuracy within 8.0 μm for a field of view of 34.0 mm × 28.4 mm, making it a reliable and precise tool for industrial applications.

Acknowledgement

The work described in this paper was mainly supported by the National Natural Science Foundation of China (No. 52375549)-China National Program and a grant from the Research Grants Council (Project No. R5047-22) of the Hong Kong Special Administrative Region, China. The authors sincerely thank the European Partnership on Metrology programme (23IND08 (DI-Vision).

References

[1] W. E. Frazier. 2014 *Journal of Materials Engineering and performance* **23** 1917-1928.

[2] B. Blakey-Milner, P. Gradl, G. Snedden, M. Brooks, J. Pitot, E. Lopez, M. Leary, F. Berto *et al.* 2021 *Materials & Design* **209** 110008.

[3] H. Xin, W. Sun and J. Fish. 2018 *International Journal of Mechanical Sciences* **149** 373-392.

[4] R. S. Mishra, R. S. Haridas and P. Agrawal. 2022 *Science and Technology of Welding and Joining* **27** 141-165.

[5] H. Yi, L. Jia, J. Ding and H. Li. 2024 *International Journal of Machine Tools and Manufacture* **194** 104103.

[6] C. Y. Yap, C. K. Chua, Z. L. Dong, Z. H. Liu, D. Q. Zhang, L. E. Loh and S. L. Sing. 2015 *Applied physics reviews* **2**.

[7] J. Li, Q. Zhou, X. Huang, M. Li and L. Cao. 2021 *Journal of Intelligent Manufacturing* 1-15.

[8] P. Lafiosca and I.-S. Fan. 2020 *Insight-Non-Destructive Testing and Condition Monitoring* **62** 692-701.

[9] Y. Wang, F. Xie, S. Ma and L. Dong. 2017 *Optics and Lasers in Engineering* **93** 164-170.

[10] N. Lazaros, G. C. Sirakoulis and A. Gasteratos. 2008 *International Journal of Optomechatronics* **2** 435-462.

[11] J. Xu and S. Zhang. 2020 *Optics and Lasers in Engineering* **135** 106193.

[12] Y. Hu, Q. Chen, S. Feng and C. Zuo. 2020 *Optics and lasers in engineering* **135** 106192.

[13] S. Feng, L. Zhang, C. Zuo, T. Tao, Q. Chen and G. Gu. 2018 *Measurement Science and Technology* **29** 122001.

[14] R. Xia, J. Zhao, T. Zhang, R. Su, Y. Chen and S. Fu. 2020 *Optik* **208** 164332.

[15] S. Matthias, M. Kästner and E. Reithmeier, "Fast in-Situ Tool Inspection Based on Inverse Fringe Projection and Compact Sensor Heads," in *Optical Metrology and Inspection for Industrial Applications IV*, 2016, vol. 10023: SPIE, pp. 87-95.

[16] Y. Zhang, W. Tao, Y. Chen, Z. Lei, R. Bai and Z. Lei. 2020 *Materials* **13** 3599.

[17] M. F. Ren, Q. Z. Huang and H. R. Chen, "Experimental Investigation into the Buckling Behavior of an Advanced Grid Stiffened Plate by a Fringe Projection Profilometry System," in *Advanced Materials Research*, 2011, vol. 217: Trans Tech Publ, pp. 1153-1158.

[18] J. Burke, T. Bothe, W. Osten and C. F. Hess, "Reverse Engineering by Fringe Projection," in *Interferometry XI: Applications*, 2002, vol. 4778: SPIE, pp. 312-324.

[19] J. Qian, S. Feng, T. Tao, Y. Hu, K. Liu, S. Wu, Q. Chen and C. Zuo. 2019 *Opt. Lett.* **44** 5751-5754.

[20] C. Jiang, S. Jia, Y. Xu, Q. Bao, J. Dong and Q. Lian. 2015 *Bio-medical materials and engineering* **26** S395-S403.

[21] A. Chatterjee, P. Singh, V. Bhatia and S. Prakash. 2019 *Optics & Laser Technology* **112** 368-378.

[22] H. L. Zhang, C. K. P. Vallabh, Y. B. Xiong and X. Y. Zhao. 2022 *Measurement* **191**.

[23] W. X. Shi, Q. Zhang, H. M. Xie and W. He. 2021 *Applied Sciences-Basel* **11**.